Academic Journal of Science and Technology
ISSN: 2771-3032 | Vol. 22, No. 1, 2026

Risk-Aware Site Selection of Transshipment Nodes for Low-Altitude Logistics Route Networks

Changke Shao, Zehua Zhang

School of Emergency Management and Safety Engineering, North China University of Science and Technology, Tangshan 063000, China

Abstract: To balance logistics efficiency and ground safety in urban low-altitude logistics, this paper proposes a risk-aware SOM-based transshipment node siting method. A 10 m static ground risk map is built to screen candidate nodes, and risk suppression and risk-gradient repulsion terms are embedded into the SOM weight update so nodes migrate to low-risk areas while fitting demand. In a 5 km x 5 km Tangshan area, at λ = 0.8 and k = 25, the average service distance rises only 1.55% (254.23 m to 258.16 m), while point risk, 50 m buffer risk, and maximum node risk fall by 17.9%, 16.5%, and 17.1%.

Keywords: UAV; logistics transportation; transshipment node site selection; SOM algorithm.

1. Introduction

With the rapid growth of e-commerce and instant delivery, low-altitude logistics UAVs are becoming a key way to relieve last-mile congestion. Transshipment nodes connect ground warehousing, regional consolidation, and last-mile demand, and their layout directly affects delivery distance, coverage, cost, and ground safety, making their location and scale a core problem for large-scale low-altitude logistics.

Existing facility location models (p-median, maximal covering, capacitated, and multi-objective) mostly optimize efficiency. In urban low-altitude logistics, however, demand concentrates in dense, high-rise core areas where UAV crashes cause greater ground damage, so demand and risk overlap strongly; efficiency-oriented models cluster nodes in high-risk areas, while strict risk constraints push them far from demand.

Previous studies locate UAV take-off/landing points, distribution centers, and transshipment nodes using covering models, GIS multi-criteria evaluation, and multi-objective optimization [1-9], and SOM has been applied to facility layout and routing [10-14]. These works mostly treat ground risk as no-fly zones or simple constraints, and classical SOM is demand-driven only, so neither can balance demand fitting with continuous ground risk.

This paper therefore proposes a risk-aware SOM (RA-SOM) method: a 10 m static ground risk map is built to obtain a feasible candidate set; the SOM weight update is reconstructed with a dynamic risk suppression term and a Gaussian-smoothed risk gradient repulsion term; and Pareto knee-point analysis determines the model parameters. Validation in the Tangshan core area shows substantial risk reduction with little efficiency loss.

2. Problem Description and Modeling

2.1. Mathematical Abstraction of Urban Low-Altitude Logistics Networks and Spatial Conflicts

In urban low-altitude logistics, a complete delivery network has three levels: trunk take-off/landing sites, regional transshipment nodes, and last-mile demand points. This paper focuses on regional transshipment node siting and layout.

Assume that, after market research and data cleaning, a set of typical demand points is extracted in the study area, denoted as $X = \{x_i \mid i = 1, 2, ..., N\}$, where each point is represented by its 2D coordinate vector $x_i \in R^2$.

The objective is to determine K transshipment node coordinates $W = \{w_j \mid j = 1, 2, ..., K\}$, where each w_j is a planned relay facility. The goal is to minimize the average service distance (ASD) from demand points to their nearest nodes, solved within the candidate feasible domain Ω:

$$\min ASD = \frac{1}{N}\sum_{i=1}^{N} \min_{j\in[1,K]} \| d_i - c_j \|_2$$
$$s.t. \quad c_j \in \Omega \quad (\forall j = 1, 2, ..., K)$$

In an ideal Euclidean plane, the ASD-minimizing solution is the spatial geometric median of demand density. Real urban space is heterogeneous and risky, so the demand density function $\rho(x)$ and the comprehensive risk function $P(x)$ show strong positive correlation and spatial overlap.

In real 3D urban space, a node C must satisfy obstacle, safety, and accessibility constraints. Based on multi-source raster data, for node c_j, the feasible domain (candidate set) Ω is defined; any node $c_j(x, y) \in \Omega$ must satisfy four constraints:

(1) Physical obstacle constraint: the location of a transshipment node must have no building obstruction at the cruise altitude set for the UAV. It must satisfy:

$$O(x_j, y_j) = 0$$

(2) Point static risk constraint: the normalized static risk $P(x_j, y_j)$ of the node's grid cell must be below the high-risk threshold P_{max}:

$$P(x_j, y_j) \le P_{max}$$

(3) Surrounding safety constraint: within a buffer of radius R, the average risk $\overline{P}_{buffer}(x_j, y_j)$ must satisfy:

$$\overline{P}_{buffer}(x_j, y_j) \le \overline{P}_{max}$$

(4) Demand accessibility constraint: the nearest demand point must not exceed the maximum last-mile delivery

threshold D_{max}:

$$\min_{i\in[1,N]} \| d_i - c_j \|_2 \leq D_{max}$$

Combining these conditions, the siting problem becomes a constrained optimization within the feasible domain Ω.

2.2. Construction of the Grid-Based Ground Static Risk Assessment Model

To quantify environmental risk, the urban physical space is discretized with GIS, and multi-source heterogeneous data (population heatmaps, POIs, building footprints, and elevation models) are rasterized.

Referring to the urban public safety risk framework [15], a 10 m ground static risk map is built, with each cell quantifying the casualty risk probability of a UAV crash.

Ground static risk depends on the UAV failure rate, crash impact range, and the exposure and vulnerability of ground elements. For a cell, the casualty probability P per flight hour is:

$$P_{risk} = p_{op} \times A \times P_e \times P_c$$

where A is the ground impact area; POP is the population density (persons/m2); Pe is the crash probability; and Pc is the mortality of affected people.

Each cell's risk factors are aggregated by multi-criteria weighted overlay into an initial risk matrix, and range normalization is applied to avoid numerical overflow and gradient explosion in later iterations.

$$P_{norm}(r,c) = \frac{P_{raw}(r,c) - \min(P_{raw})}{\max(P_{raw}) - \min(P_{raw}) + \grave{o}}$$

where $P_{raw}(r,c)$ is the raw absolute risk at grid (r,c); $\min(P_{raw})$ and $\max(P_{raw})$ are the global minimum and maximum risk; and $\grave{o}$ is a small bias constant preventing division by zero.

Because UAV operation is environment-dependent, building outlines above the operating altitude are overlaid into a binarized obstacle matrix O, the hard constraint for candidate screening.

3. Solution Algorithm

For the efficiency-safety conflict, hard no-fly-zone models produce infeasible or marginalized layouts, while classical SOM is demand-driven only. This study reconstructs the SOM weight update by embedding a risk-aware dual-driving model.

3.1. Pre-screening of the Candidate Transshipment Node Set Ω

Before RA-SOM runs, a feasible candidate set Ω is generated by pre-screening the urban raster base map:

1. Physical obstacle filtering: remove the center points of all cells with O = 1.

2. Safety red-line filtering: remove cells whose point risk $P > 0.8.$ and 50 m buffer risk $\overline{P} > 0.5$ exceed the safety thresholds.

3. Service gap filtering: remove isolated cells farther than 800 m from the nearest demand point. The candidate set Ω is the physical reference space for neuron placement.

3.2. Classical SOM Algorithm Foundation and Isomorphic Mapping to the Site-Selection Scenario

Classical SOM is an unsupervised competitive network that preserves topology, and its competition is spatially analogous to transshipment node siting.

The two SOM layers are given clear spatial meanings:

(1) Input layer: the input samples are the 2D coordinates $X = x_i | i = 1,2,\dots,N$ of all demand points, where $x_i \in R^2$ is the coordinate vector of one demand point; one point is randomly drawn each iteration to drive the competition.

(2) Competitive layer: a grid of K neurons (K equals the planned node number), each with an updatable 2D weight vector $w_j \in R^2 (j = 1,2,\dots,K)$; in siting, w_j is the surface projection coordinate of a transshipment node.

The core competitive process is:

(1) Best matching unit: for demand sample x_i, the neuron with the smallest Euclidean distance to it is the BMU:

$$BMU(x_i) = \arg \min_{j\in[1,K]} |x_i - w_j|_2$$

(2) Weight update: the BMU and its neighbors are driven toward the demand sample to fit the demand distribution, with the basic update $w_j(t+1) = w_j(t) + \eta(t) \cdot h_{j,BMU}(t) \cdot \left(x_i - w_j(t)\right)$

where t is the iteration number, $\eta(t)$ is the decaying learning rate, and $h_{j,BMU}(t)$ is the Gaussian neighborhood function.

3.3. Inherent Deficiencies of Classical SOM in Low-Altitude Logistics Site Selection

Classical SOM has three key deficiencies for low-altitude siting:

(1) No risk perception: neurons only fit demand and cluster in high-risk areas, increasing ground risk exposure.

(2) Hard constraints break convergence: post hoc removal or hard boundaries cause infeasible or edge-biased suboptimal layouts.

(3) Existing improvements (e.g., LASOM) only improve coordinate fidelity without embedding the risk field.

3.4. Bottom-Level Reconstruction of the RA-SOM Risk-Aware Mechanism

To overcome these deficiencies, the weight update is improved with a risk-aware dual-driving mechanism.

The reconstructed RA-SOM weight update is: $w_j(t+1) = w_j(t) + \eta(t) \cdot h_{j,BMU}(t) \cdot \left[\left(1 - \lambda \cdot P\left(w_j(t)\right)\right) \cdot \left(x_i - w_j(t)\right) - \lambda \cdot P\left(w_j(t)\right) \cdot \nabla P_{smooth} \cdot S\right]$

where $\lambda \in [0,1]$ is the global risk preference weight; $P\left(w_j(t)\right)$ is the normalized static risk, at iteration t, of the cell of neuron w_j; ∇P_{smooth} is the smoothed risk gradient; and S is the spatial scale factor.

RA-SOM updates weights in the continuous plane for refined optimization; after iteration, the neuron coordinates are mapped back to the discrete candidate set Ω.

(1) Global state control function

Learning rate: $\eta(t) = \eta_{init} \cdot (1 - t/T_{max})$, where η_{init} is the initial rate and T_{max} the maximum iterations.

Neighborhood function: $h_{j,BMU}(t) = \exp\left(-\frac{|w_j - w_{BMU}|_2^2}{2\sigma^2(t)}\right)$, with radius $\sigma(t) = \sigma_{init} \cdot \exp\left(-t/(T_{max}/4)\right)$; the neighborhood shrinks from global exploration to single-node fine adjustment.

(2) Dynamic risk suppression centripetal term

In the formula, $\left(1-\lambda \cdot P\left(w_j(t)\right)\right) \cdot \left(x_i - w_j(t)\right)$ is the risk suppression centripetal term and $\left(1-\lambda \cdot P\left(w_j(t)\right)\right)$ is the adaptive damping coefficient that blocks demand attraction from high-risk areas.

When the neuron is in a high-risk area ($P\left(w_j(t)\right) \to 1$) with strong risk avoidance (large λ), the damping decays to near 0, preventing nodes from being pulled into high-risk demand areas.

When the neuron is in a low-risk area ($P\left(w_j(t)\right) \to 0$), the damping approaches 1, preserving demand fitting and coverage.

(3) Gaussian-smoothed risk gradient repulsion term

In the formula, $-\lambda \cdot P\left(w_j(t)\right) \cdot \nabla P_{smooth} \cdot S$ is the repulsion term that actively drives neurons out of high-risk areas.

Direct gradient on the 10 m raster causes oscillation; the map is smoothed by a 5 x 5 (50 m) Gaussian filter to obtain the field P_{smooth}, then the gradient ∇P_{smooth} is computed by finite differences.

In a high-risk area ($P\left(w_j(t)\right) \to 1$), the repulsion drives the neuron along the fastest gradient descent to low-risk depressions.

In a low-risk area ($P\left(w_j(t)\right) \to 0$), the repulsion tends to 0 and does not affect convergence.

3.5. Complete Iterative Process of the RA-SOM Algorithm

1. Data preparation: load the risk map and demand points X, and generate the candidate set Ω.

2. Initialization: within the study area, randomly initialize, for K neurons, the weight vectors w_j.

3. Competition and update: run T_{max} iterations; draw a demand point x_i, find the BMU, and update weights by the reconstructed formula in Section 3.4.

4. Spatial snapping: for each neuron coordinate $w_j^* \in R^2$, search the candidate set Ω for the closest feasible coordinate $\hat{c}_j$:

$$\hat{c}_j = \arg\min_{c \in \Omega} \| w_j^* - c \|_2$$

5. Output: the snapped coordinate set $\hat{C} = \{\hat{c}_1, \ldots, \hat{c}_K\}$ is the final siting scheme.

Table 1. Core global configuration parameters of the RA-SOM model

Parameter name (variable code)	Physical meaning and description	Setting value / range
GRID_RES	Absolute spatial resolution of the grid system	10 m
T_max (NUM_ITER)	Maximum total number of neural network training iterations	5000
GRAD_SIGMA	Risk gradient smoothing coefficient	3
SPATIAL_SCALE_RATIO	Spatial scale conversion coefficient	0.08
η_init (LEARNING_RATE)	Initial maximum base learning rate	1.5
σ_init (SIGMA_INIT)	Initial maximum Gaussian neighborhood radius	1.5
λ (RISK_WEIGHT)	Global risk preference weight coefficient	[0,1]
X_min/X_max, Y_min/Y_max	Geographic boundary of plane coordinates of the study area	Dynamically obtained

4. Case Study and Validation

4.1. Simulation Environment

Using OpenStreetMap data, a 5 km x 5 km Tangshan area is modeled and rasterized into 250,000 cells; there are 124 demand points, and the data sources are listed in Table 2.

Table 2. Data sources

Data type name	Data spatial accuracy and format	Main source basis
Population density data	100 m planar resolution, GeoTIFF raster format	WorldPop open dataset, China kilometer grid population distribution data
Urban 3D building and elevation data	Vector polygon data with height and footprint attribute fields	Extracted from OpenStreetMap (OSM) open vector data
POI data	Vector point data (CSV/JSON) with coordinates and labels	Batch collection from the Amap open platform POI data interface

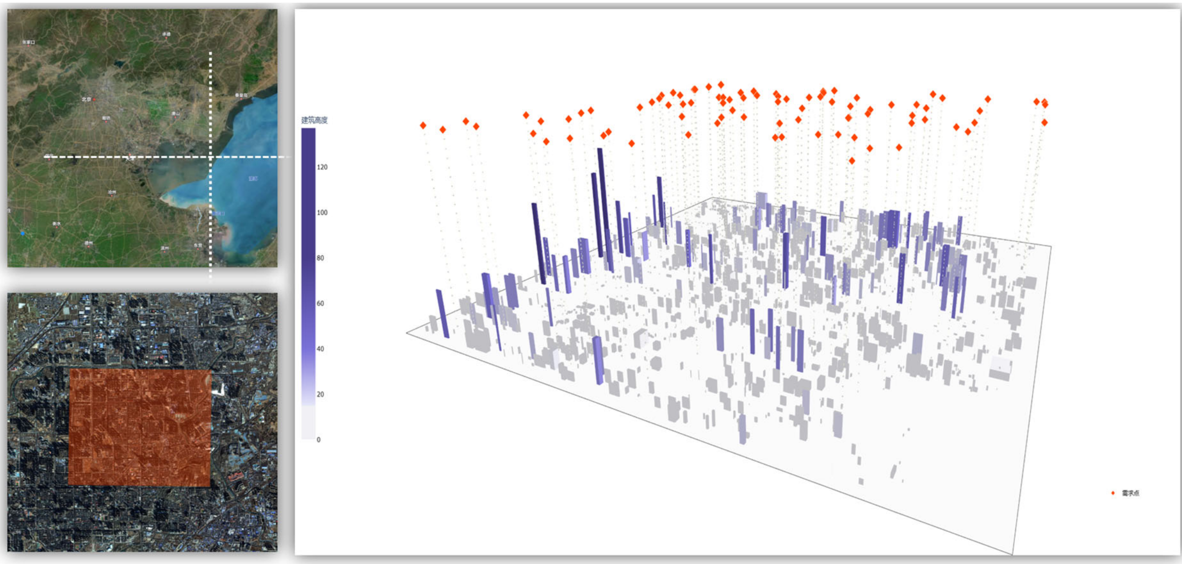

Figure 1. Schematic diagram of the study area

4.2. Generation of the Ground Risk Base Map

The simulation environment is built in Python with the SF Fengyi Ark 80 UAV; key parameters are:

$\omega_1 = 0.3, \omega_2 = 0.7, V_0 = 23\mathrm{m/s}, m = 30\mathrm{kg}, g = 9.8\mathrm{m/s^2}$, $C_D = 0.4$, $\rho_{air} = 1.29\mathrm{kg/m^3}$, $A_x = 0.486\mathrm{m^2}$, $A_z = 0.122\mathrm{m^2}, P_e = 7.23 \times 10^{-6}$.

Integrating no-fly, obstacle, and special-zone layers with the ground risk model, the ground personnel risk layer is generated according to population density and shielding effects, as shown in the figure.

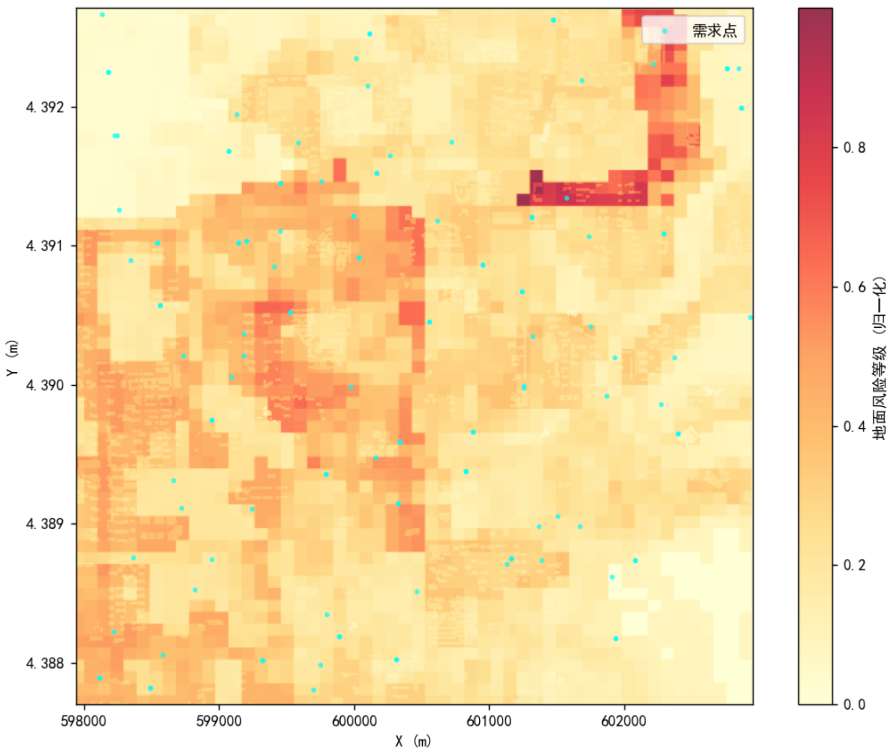

Figure 2. Multi-source data risk base map

4.3. Multi-Objective Optimization Based on the Pareto Frontier and Determination of the Optimal Risk Preference Coefficient

To calibrate λ, 11 equally spaced experiments are run over $\lambda \in [0,1]$ to build the Pareto frontier from node average risk and whole-network ASD.

As λ increases, node risk decreases exponentially while ASD rises linearly. The geometric knee-point method is used to remove subjective bias:

Both indicators are range-normalized, and the frontier point closest to the ideal zero point is the optimal balance.

The knee point is $\lambda = 0.8$: below it, small λ gains greatly improve safety with little ASD increase; above it, safety gains are marginal while ASD rises sharply.

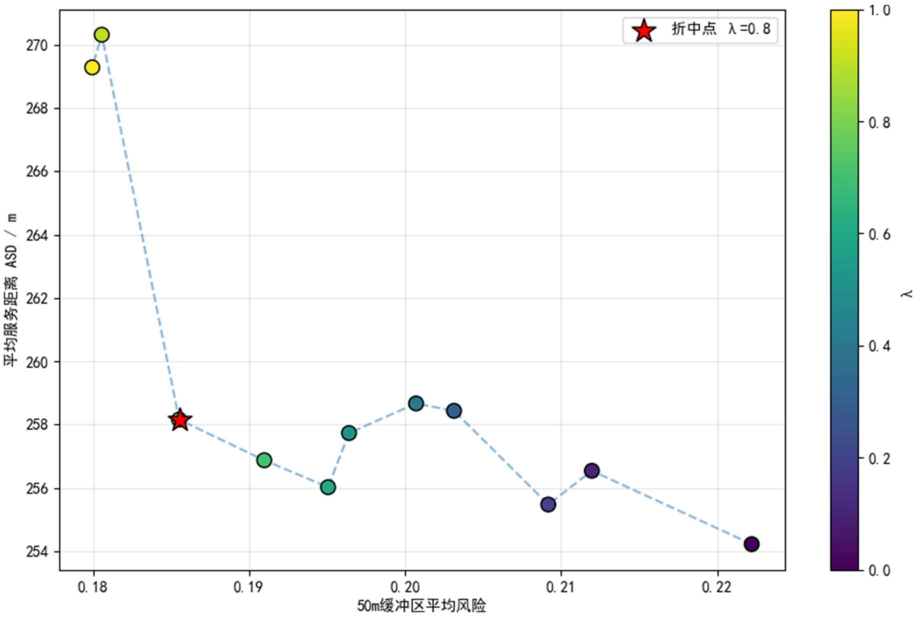

Figure 3. Pareto frontier

4.4. Determination of the Optimal Deployment Scale

The node scale k is constrained by land cost, airspace capacity, and budget; density over 2 nodes/km (k > 50) causes severe route overlap, so k is limited to [2, 49].

The geometric knee-point method identifies the scale-efficiency knee point:

(1) Range-normalize the node scale and ASD sequences.

(2) Form the reference chord L from the efficiency upper-bound points.

(3) The sampling point with the largest orthogonal distance to L is the knee point.

The knee point is k = 25: below it, adding nodes sharply reduces ASD; above it, gains narrow and costs rise rapidly.

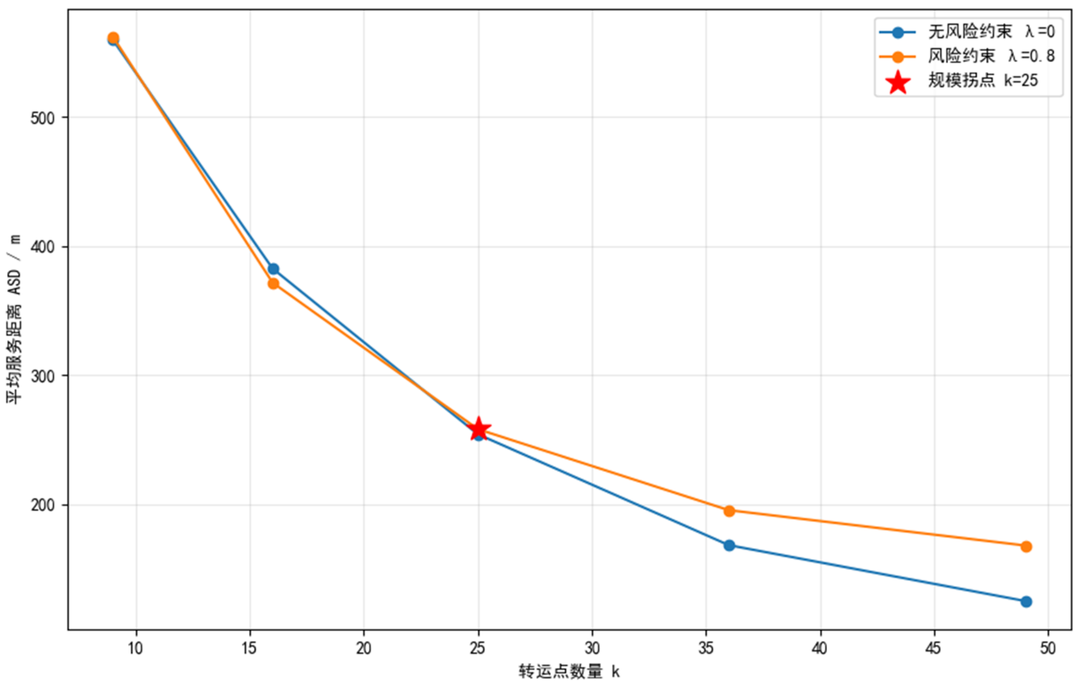

Figure 4. Scale-efficiency curve analysis

4.5. Performance Validation of the Final Scheme

Final validation uses the optimal parameters ($\lambda = 0.8$, $k = 25$) and compares with the baseline without risk constraints ($\lambda = 0.0$) (Table 3). ASD rises only from 254.23 m to 258.16 m (1.55%), while average point risk falls 17.9% (0.216 to 0.177) and maximum node risk falls 17.1% (0.527 to 0.437).

Risk-driven nodes migrate on average 123.39 m (up to 484.15 m), verifying that the model moves nodes to low-risk areas while maintaining coverage.

Table 3. Comparison of core performance indicators of different schemes

Scheme type	Deployment scale k	Risk preference λ	Average service distance ASD (m)	Average node point risk	Maximum node risk	Average node migration distance (m)
Baseline scheme without safety constraints	25	0.0	254.23	0.2156	0.5267	0.00
Strong safety-constrained scheme	25	0.8	258.16	0.1769	0.4367	123.39

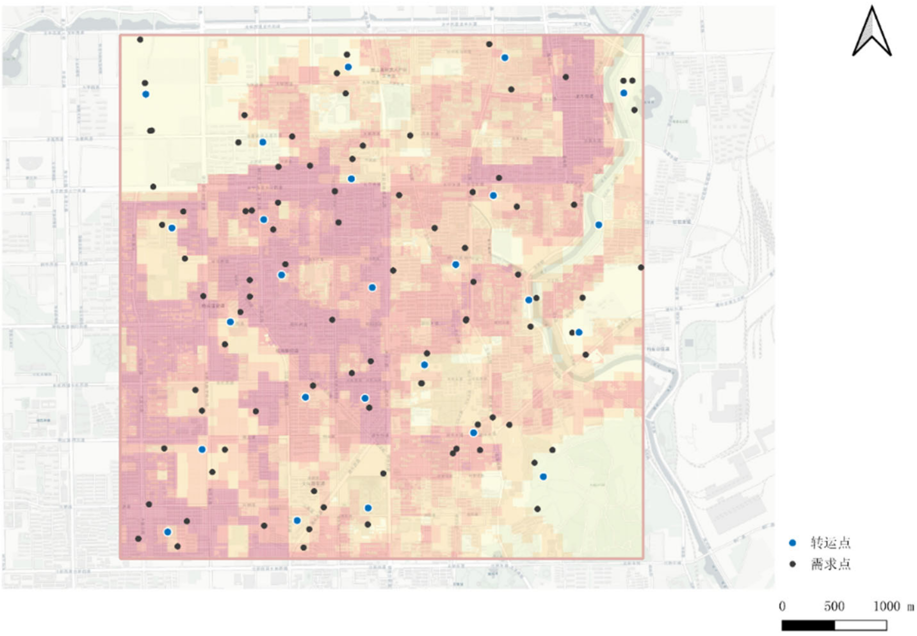

Figure 5. Final transshipment node layout

5. Conclusion

The RA-SOM siting method was proposed and validated in the Tangshan core area. Main conclusions:

(1) A spatial constraint system combining obstacle avoidance and risk quantification was built from 10 m population, building, and POI data.

(2) The SOM weight update was improved with dynamic risk suppression and Gaussian-smoothed risk gradient repulsion, enabling nodes to migrate to low-risk areas.

(3) At $\lambda = 0.8$ and $k = 25$, ASD rises only 1.55% while point, 50 m buffer, and maximum risk fall 17.9%, 16.5%, and 17.1%.

(4) Risk gradients drive average node migration of 123.39 m (maximum 484.15 m), supporting low-altitude network planning.

References

[1] Jia, Y., Su, Y., & Wang, Y. (2023). Improved immune algorithm for sudden cardiac death first aid drones site selection. International Journal of Medical Informatics, 173, 105025. https://doi.org/10.1016/j.ijmedinf.2023.105025.

[2] Kim, M., Hong, W., Lee, Y., & Baek, S.-C. (2022). Selection of take-off and landing sites for firefighter drones in urban areas using a GIS-based multi-criteria model. Drones, 6(12), 412. https://doi.org/10.3390/drones6120412

[3] Shavarani, S. M., Golabi, M., & Izbirak, G. (2021). A capacitated biobjective location problem with uniformly distributed demands in the UAV-supported delivery operation. International Transactions in Operational Research, 28(6), 3220-3243. https://doi.org/10.1111/itor.12735

[4] Li, Z., Li, S., Lu, J., & Zhang, H. (2025). Air route network planning method of urban low-altitude logistics UAV with double-layer structure. Drones, 9(3), 193. https://doi.org/10.3390/drones9030193

[5] Li, Z. P., & He, Y. M. (2024). Site selection of UAV take-off and landing points in complex mountainous environments based on a combined GA-SA algorithm. Science Technology and Engineering, 24(02), 850-857.

[6] Liu, G. C., & Ma, Y. S. (2023). Research on location and task assignment of urban logistics UAV distribution centers. Flight Dynamics, 41(03), 88-94.

[7] Yang, H. Y., Li, Y. F., & Duan, M. Z. (2025). Site selection and path planning of urban logistics UAV take-off and landing

points. Science Technology and Engineering, 25(28), 12130-12138.

[8] Yang, J. T., & Li, Z. P. (2025). Maximum coverage model site selection of urban UAV take-off and landing sites based on spatially continuous demand. Science Technology and Engineering, 25(11), 4793-4800.

[9] Li, Z. L., Li, S., & Zhang, H. H. (2026). Three-dimensional route network planning method for urban low-altitude logistics UAVs. Journal of Traffic and Transportation Engineering, 26(04), 50-67.

[10] Schwardt, M., & Dethloff, J. (2005). Solving a continuous location-routing problem by use of a self-organizing map. International Journal of Physical Distribution & Logistics Management, 35(6), 390-408. https://doi.org/10.1108/09600030510608315

[11] Leung, E. K. H., Das, S., & Bektaş, T. (2025). Optimizing delivery systems within the e-retail context: a weighted self-organizing map for delivery region partitioning. European Journal of Operational Research.

[12] Xu, L., Zhu, Z., Hu, Z., & Zhang, Q. (2025). A study on UAV path planning for navigation mark inspection using two improved SOM algorithms. Journal of Marine Science and Engineering, 13(8), 1537. https://doi.org/10.3390/jmse13081537

[13] Jiang, R., Fan, S. W., & Wang, X. M. (2025). Clustering algorithm based on improved SOM network. Computer Science, 52(08), 162-170.

[14] Zhang, X. X. (2021). Research on emergency facility location based on the importance of urban traffic network nodes [Master's thesis]. Shijiazhuang Tiedao University.

[15] Zhang, L. Y., Zhang, Z. H., Wang, Q. Q., & Chen, L. (2026). Research on urban low-altitude route planning based on ground risk. Flight Dynamics, 44(03), 88-95.